33rd Annual International Conference of the IEEE EMBS
Boston, Massachusetts USA, August 30 - September 3, 2011

Change detection and classification in brain MR images using Change Vector Analysis

Rita Simões and Cornelis Slump

Abstract— **The automatic detection of longitudinal changes in brain images is valuable in the assessment of disease evolution and treatment efficacy. Most existing change detection methods that are currently used in clinical research to monitor patients suffering from neurodegenerative diseases—such as Alzheimer's—focus on large-scale brain deformations. However, such patients often have other brain impairments, such as infarcts, white matter lesions and hemorrhages, which are typically overlooked by the deformation-based methods. Other unsupervised change detection algorithms have been proposed to detect tissue intensity changes. The outcome of these methods is typically a binary change map, which identifies changed brain regions. However, understanding what types of changes these regions underwent is likely to provide equally important information about lesion evolution. In this paper, we present an unsupervised 3D change detection method based on Change Vector Analysis. We compute and automatically threshold the Generalized Likelihood Ratio map to obtain a binary change map. Subsequently, we perform histogram-based clustering to classify the change vectors. We obtain a Kappa Index of 0.82 using various types of simulated lesions. The classification error is 2%. Finally, we are able to detect and discriminate both small changes and ventricle expansions in datasets from Mild Cognitive Impairment patients.**

I. INTRODUCTION

The automatic detection of longitudinal changes in images of the brain has found applications in several neurological diseases, such as tumours and Multiple Sclerosis (MS), with the aim of assessing disease evolution and treatment efficacy [1]. In neurodegenerative diseases, such as Alzheimer's Disease (AD), most change detection methods can detect large-scale brain deformations. Tensor-Based Morphometry (TBM) has been extensively used in longitudinal and cross-sectional studies of Mild Cognitive Impairment (MCI) and AD populations [2]. In single-subject longitudinal analyses, TBM consists of warping a follow-up image into the baseline image such that the differences between the two images are cancelled out. The Jacobian (determinant of the Jacobian matrix) of the resulting deformation field is computed afterwards, giving information about local volume loss or gain [3]. However, the major disadvantage of TBM is that it is based entirely on the analysis of the deformation field, which is largely influenced by the registration techniques used and parameters chosen [4]. Non-linear registration methods are highly under-constrained, meaning that for a given pair of images there is a large number of possible displacement fields. In addition, almost all non-linear registration methods require an intensity correspondence between two homologous voxel areas in the images. This necessitates an assumption that a certain region of the brain is present in both images at a similar intensity, only at a different position in each image [1], [3].

Furthermore, AD and MCI patients are likely to have other types of lesions, which should also be carefully evaluated and monitored. White-matter lesions (WMLs), characterized by lower signal intensities in T1-weighted images and higher intensities in T2-weighted images, are known to often occur in these patients [5]. Perfusion [6] and diffusion [7] impairments, such as infarcts or hemorrhages, have also been reported. These lesions—besides often influencing the outcome of the non-linear registration method—are not detected by TBM methods.

Over recent years, several unsupervised change detection algorithms have been proposed in a large variety of scientific areas, such as video surveillance, remote sensing, driver assistance systems and medical imaging [8]. In the field of neuroimaging, change detection algorithms are often used for detecting small changes. Bosc *et al.* [9] described a complete framework for change detection in MS lesions using multimodal MR images taken at several time points over a two-year period. Because the aim was to detect small changes, the preprocessing of the images included a coarse non-linear registration of the follow-up images into the baseline image, in order to cope with large deformations. More recently, Seo and Milanfar [10] used local steering kernels as features to compute the dissimilarity between a baseline and a follow-up image. They used only one MRI modality and applied the method to small simulated 2D lesions.

These approaches result in binary change maps, which show only where a change has occurred. However, knowing how the tissue has evolved might be as important as identifying its location. For example, an infarct might not change volume but the tissue may be recovering, as shown by altered T1 and/or T2 intensities. Patriarche *et al.* [11] proposed an algorithm for the automatic assessment of tumour evolution that detects and categorizes changes in intensities. However, its applicability is limited to brain tumours due to the use of a specific classification system. Lemieux used the difference image of two T1 images and classified the changed pixels as signal increasing or decreasing [12].

In this work, we propose an unsupervised change detection method to detect both large-scale deformations and small and

This work is part of the VIP-BrainNetworks project, which is funded by the department of Economic Affairs of the Netherlands and the provinces of Gelderland and Overijssel.

R. Simões and C. Slump are with the Signals and Systems Group, Faculty of Electrical Engineering, Mathematics and Computer Science, University of Twente, 7500 AE Enschede, The Netherlands A.R.Lopessimoes@ewi.utwente.nl

subtle lesions while also classifying the types of detected changes. Our approach is based on Change Vector Analysis (CVA) applied to multimodal (T1- and T2-weighted) MR images. CVA is already widely used in remote sensing to evaluate changes in, for example, satellite images. For each voxel characterized by m features, the respective change vector (CV) is defined as the difference between the follow-up and the baseline feature vectors. In its basic form, the change vector's magnitude represents how much the respective voxel has changed in intensity. In turn, its direction is related to the type of change the voxel has undergone [13].

We present a modified CVA method, in which a change map is initially computed using the Generalized Likelihood Ratio Test [14]. Subsequently, the changes found are classified according to their respective CV angles. We evaluate the algorithm by simulating lesions of different types, *i.e.*, T1 and/or T2 increasing/decreasing. Additionally, we test our method in two MRI datasets from MCI patients. All the processing is performed three-dimensionally.

The rest of this paper is organized as follows. Firstly, Section II describes the datasets that are used, the preprocessing steps and the proposed change detection method. Next, the results, both for simulated lesions and for real datasets, are presented and discussed. Finally, some conclusions and recommendations for further work are given in Section IV.

II. METHODS

A. Data

Three-dimensional MR images are utilized in this study. The datasets are retrieved from a large database of a cognition study with MCI patients carried out in the University Hospital of Essen, Germany. The patients are scanned at baseline and two years after presenting with MCI at the hospital. Each evaluation consists of two MRI modalities (T1- and T2-weighted). The images were acquired using an MRI scanner (Siemens Avanto, 1.5 T). The following protocols were used: 3D T1-weighted (TR/TE = 40/5 ms; acquisition matrix = [256 256]; 176 slices; voxel size = 1.016 mm $\times$ 1.016 mm $\times$ 1 mm) and 3D T2-weighted (TR/TE = 3200/416 ms; acquisition matrix = [256 230]; 192 slices; voxel size = 1.016 mm $\times$ 1.016 mm $\times$ 1 mm).

B. Preprocessing

Before applying a change detection method to a set of longitudinal images, a preprocessing stage must be applied in order to compensate for acquisition differences, such as the position of the patient, the presence of bias field inhomogeneities and intensity differences. The preprocessing pipeline is carried out using FSL tools (FMRIB Software Library, www.fmrib.ox.ac.uk/fsl) [15], except for the final step, and consists of the following four steps:

1) Skull-constrained within-modality affine registration - we follow the registration framework utilized in SIENA (Structural Image Evaluation, using Normalisation, of Atrophy, http://www.fmrib.ox.ac.uk/fsl/siena), which uses the skulls to constrain the affine registration [16].
2) Between-modalities affine registration - the T2 baseline image after within-modality registration is registered to the T1 baseline image. The resulting transform is applied to the T2 follow-up image. After this step, all four images are in the same reference space.
3) Brain extraction and bias field correction - the brain is segmented using BET (Brain Extraction Tool, http://www.fmrib.ox.ac.uk/fsl/bet2) [17] and corrected for bias field inhomogeneities with FAST (FMRIB's Automated Segmentation Tool, http://fsl.fmrib.ox.ac.uk/fsl/fast4/) [18].
4) Intensity normalization - the histograms of the follow-up images are matched to those of the respective baseline images, by using ITK [19].

These steps are shown schematically in Fig. 1.

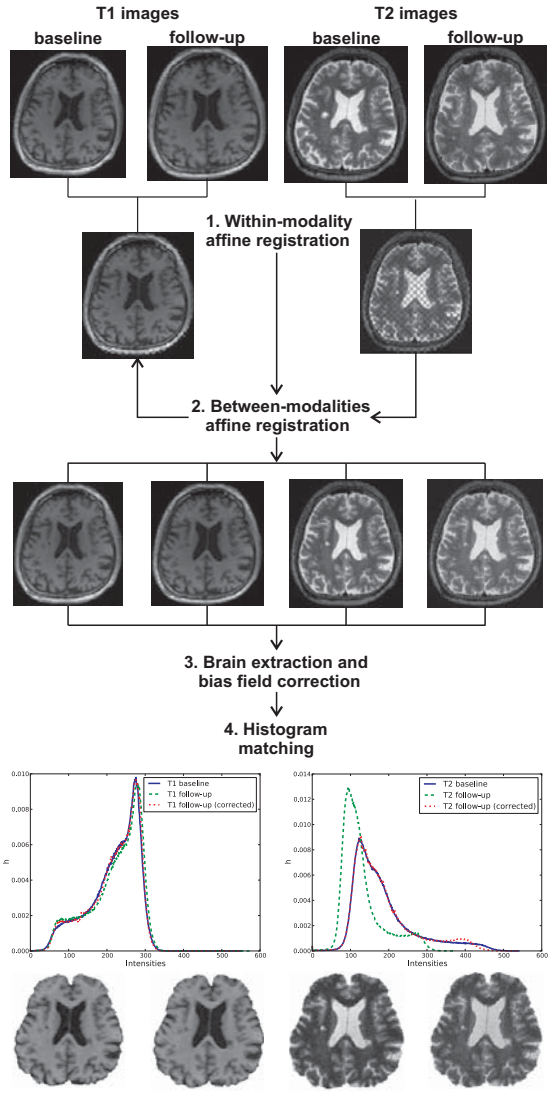

Fig. 1. Preprocessing pipeline. See text for an explanation of each step.

C. Change detection and classification

A change vector (CV) is defined as the difference between the follow-up and the baseline feature vectors (1). The

features used in this work are the T1 and the T2 intensities, as shown in Fig. 2.

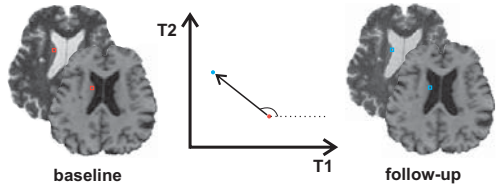

Fig. 2. Change vector for a T2-increasing and T1-decreasing change.

$$\mathbf{CV} = \mathbf{I}_f - \mathbf{I}_b \tag{1}$$

with $\mathbf{I}_f$ and $\mathbf{I}_b$ being the voxel's intensity vector at follow-up and baseline, respectively.

The change vector is characterized by a magnitude and an angle:

$$\|\mathbf{CV}\| = \sqrt{{CV_{T_1}}^2 + {CV_{T_2}}^2} \tag{2}$$

$$\angle\mathbf{CV} = \arctan\left(\frac{CV_{T_2}}{CV_{T_1}}\right) \tag{3}$$

Typically, the change vector magnitude is used to determine the binary change map. Instead of using the magnitude of the change vector, which has been reported to be sensitive to noise, intensity inhomogeneities and registration errors, we use the Generalized Likelihood Ratio (GLR) test [14], defined for multimodal images in [9], in order to assess whether a change has occurred (H_1 hypothesis) or not (H_0 hypothesis). The test is performed voxelwise within a $3\times3\times3$ local window W. The GLR assumes Gaussian-distributed intensities. It corresponds to the ratio between $p(H_1)$ and $p(H_0)$ and is defined as [9]:

$$\begin{aligned} GLR_s = -\frac{1}{2}\sum_{i\in W_s} [&(I_b(i)-\widehat{\mu}_b)^T\mathbf{C}^{-1}(I_b(i)-\widehat{\mu}_b)+ \\ &(I_f(i)-\widehat{\mu}_f)^T\mathbf{C}^{-1}(I_f(i)-\widehat{\mu}_f)- \\ &(I_b(i)-\widehat{\mu}_0)^T\mathbf{C}^{-1}(I_b(i)-\widehat{\mu}_0)- \\ &(I_f(i)-\widehat{\mu}_0)^T\mathbf{C}^{-1}(I_f(i)-\widehat{\mu}_0)] \end{aligned} \tag{4}$$

where $\mathbf{C}$ is the covariance matrix of the noise image, calculated as in [9], and $\widehat{\mu}_{0,b,f}$ are the mean estimators determined as in [14] for the two hypotheses.

In order to obtain a change map, the GLR must be thresholded. Considering the histogram of the change maps obtained at small (Fig. 3a and Fig. 3b) and at high threshold values (Fig. 3c and Fig. 3d), two observations can be pointed out. Firstly, at a small threshold the histogram is almost uniform; in contrast, the histogram obtained with a high threshold shows clearly distinguishable peaks. Secondly, an offset is present in the case of the low threshold value, while the high threshold histogram has a zero baseline. We decide on the threshold value based on the histogram offsets of change maps computed at increasing threshold values (Fig. 4a). The offset is calculated as the mean value of the histogram in unchanged regions. We obtain these regions by computing a piecewise linear approximation of the histogram at intervals of 20^o. The unchanged regions are then taken as the three intervals with the flattest linear fit. Finally, the threshold is selected when the offset becomes lower than 0.0003 - horizontal line in Fig. 4a). This value was selected empirically so as to be small but still larger than zero.

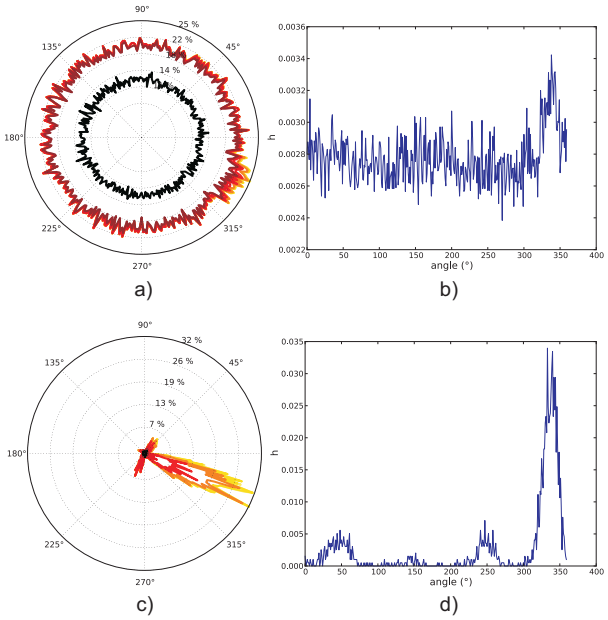

Fig. 3. Angular histograms of the change vectors obtained after thresholding the GLR map with: a) and b) a low threshold; c) and d) a high threshold. In a) and c), different line colors correspond to different change vector magnitude bins.

After thresholding the GLR map, the changed voxels are clustered based on their angular histograms. A Parzen density estimator is used to obtain a smooth approximation of the angular histogram. The local maxima and minima of the estimated curve are detected (Fig. 4b). An angle cluster is then defined as being centered on a local maximum and contained within two local minima. After clustering, the detected lesions can be inspected in a polar plot (Fig. 4c).

III. RESULTS

A. Simulated lesions

To evaluate the change detection method's performance, we simulate lesions of various sizes and intensities on Patient #1's baseline image. Eight distinctive lesions are simulated as in [20] and combined into several groups of two, three or four lesions. Various T1 and T2 intensities are assigned to each lesion, ranging from 5% to 40% increase/decrease with respect to the baseline intensities. Gaussian noise (2% of the brain's intensity range) is then added to the resulting image.

In total, 40 simulations are carried out. Our evaluation is two-fold: first we calculate the Kappa Index (Equation 5) to assess how close our binary change map (CM) is to the ground truth (GT); afterwards, we determine the classification error, which we define as the percentage of voxels that were correctly classified as "changed voxels" but were incorrectly assigned to a lesion type.

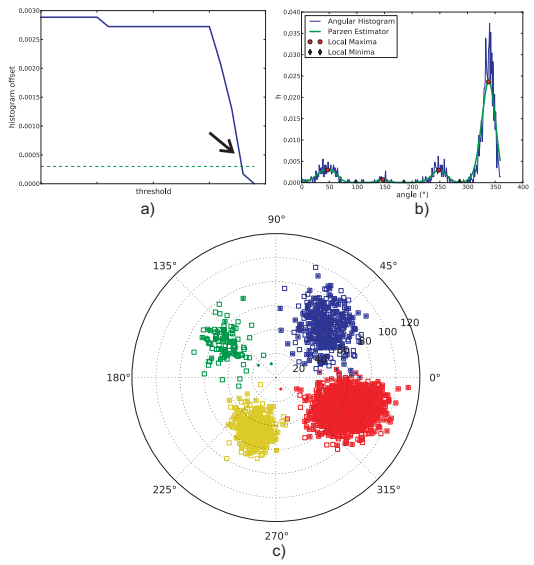

Fig. 4. a) Evolution of the angular histogram's offset with varying thresholds; the selected threshold is pointed by the arrow. b) Angular histogram with its Parzen estimation, local maxima and minima. c) Polar plot of the change vectors after clustering; squares represent the ground truth and dots refer to the detected lesions; different colors correspond to different simulated/detected lesions.

$$KI = 2\frac{\#(GT \bigcap CM)}{\#GT + \#CM} \tag{5}$$

A KI of 1 corresponds to a perfect agreement between real and calculated change maps. Altman *et al*. consider that KI values within the range 0.60-0.80 correspond to a "good" matching [21]. Bartko *et al*. observed that KI values greater than 0.70 are generally regarded as an "excellent" agreement between detection results and ground truth [22]. In our experiments, we obtained an average KI of 0.82 and an average classification error of 2%.

B. Mild Cognitive Impairment Data

Fig. 5 shows the results obtained for the first dataset. Three different types of changes were detected: the larger one, in green, corresponds to ventricular expansion; in red, a T1-increasing and T2-decreasing change, in the deep white matter, which suggests an improvement in the previously existing lesion (outlined in Fig. 6); finally, a T2-increasing change was detected near the brainstem.

The results for Patient #2 are shown in Fig. 7. Besides expansion of the ventricles (in green), two other change types were detected. These are related to an intraventricular abnormality (possibly a hemorrhage), as is clear from inspecting the baseline and follow-up T2 images (Fig. 8). The T1 images do not show such differentiated intensities in this region, which explains why the respective CV angles are around 90^o and 270^o.

IV. CONCLUSIONS AND RECOMMENDATIONS

In this paper, we have presented an unsupervised method to detect and discriminate changes in longitudinal images of the brain. Using simulated lesions, we obtained a Kappa Index of 0.82 and a classification error of 2%. Our preliminary

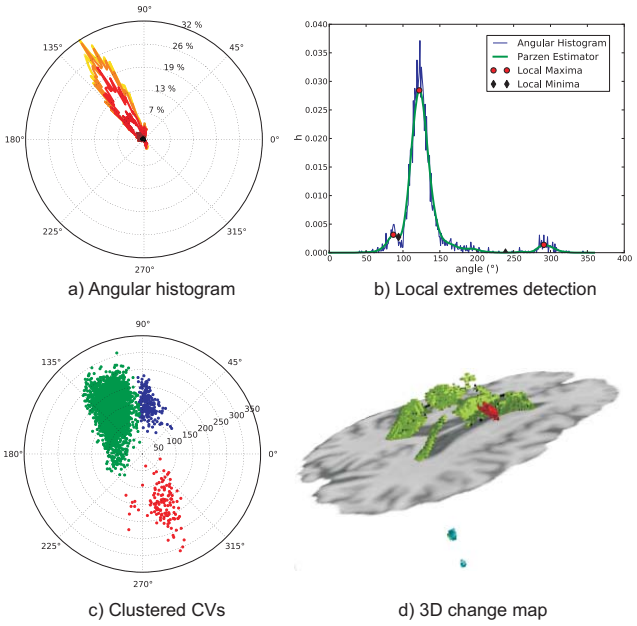

Fig. 5. Change detection in Patient #1.

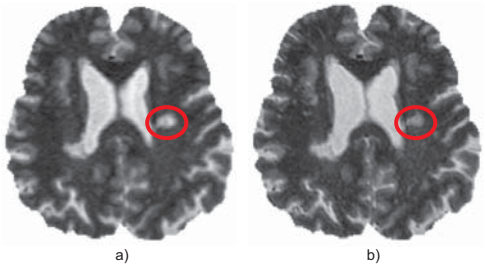

Fig. 6. Baseline (a) and follow-up (b) T2 slice from Patient #1, with the changing lesion outlined.

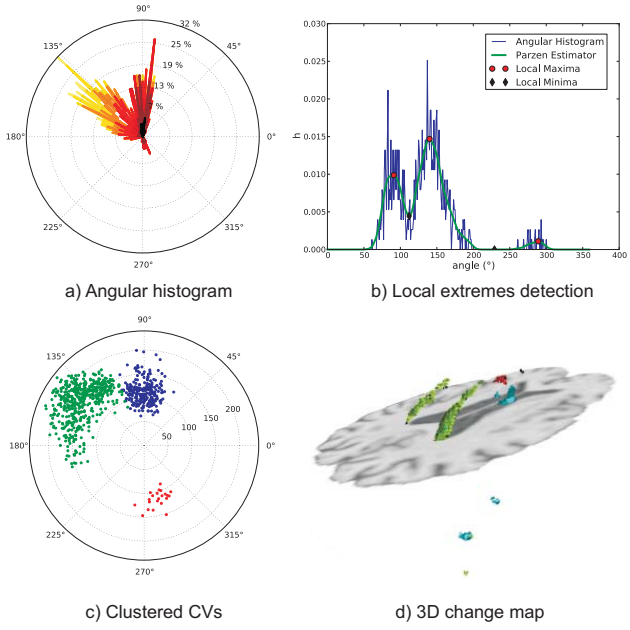

Fig. 7. Change detection in Patient #2.

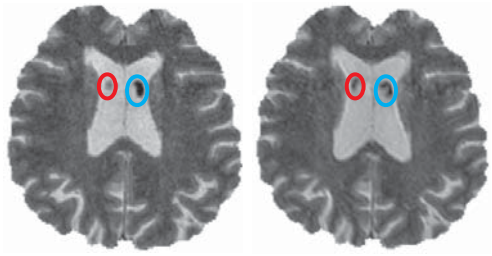

Fig. 8. Baseline (a) and follow-up (b) T2 slice from Patient #2, with the two changes outlined.

results have further demonstrated that the method is able to identify both ventricular enlargement and the evolution of small and subtle lesions in MCI subjects.

However, the method has several drawbacks. Even though a local window was taken to compute the change map—thereby diminishing the influence of possible local misregistration errors—the sensitivity of the method to such errors was not assessed. The same applies to the intensity corrections and normalisations. A thorough study into the sensitivity of the algorithm to the preprocessing steps is therefore highly desirable to allow improvement of the discrimination between artifacts and actual changes. The need for such study is even greater in the absence of a ground truth, although that is true of most longitudinal imaging studies.

Furthermore, other features, such as texture descriptors, image gradient and Laplacian, also need to be considered so as to include more information about tissues' local properties. In that case, other angle measures would have to be used, such as the generalized direction cosines.

Finally, the method's performance must be evaluated against a larger database with more types of lesions. Ultimately, our goal is to develop a general, automatic and robust change detection method that can be applied to the diagnosis and monitoring of a variety of neurological diseases.

V. ACKNOWLEDGMENTS

The authors gratefully acknowledge the University Hospital of Essen for providing the MCI datasets used in this study.

REFERENCES

[1] J. Patriarche and B. Erickson, "A review of the automatic detection of change in serial imaging studies of the brain," *Journal of Digital Imaging*, vol. 17, pp. 158–174, 2004.

[2] X. Hua, A. D. Leow, S. Lee, A. D. Klunder, A. W. Toga, N. Lepore, Y. Chou, C. Brun, M. Chiang, M. Barysheva, C. R. Jack, M. A. Bernstein, P. J. Britson, C. P. Ward, J. L. Whitwell, B. Borowski, A. S. Fleisher, N. C. Fox, R. G. Boyes, J. Barnes, D. Harvey, J. Kornak, N. Schuff, L. Boreta, G. E. Alexander, M. W. Weiner, P. M. Thompson, and Alzheimer's Disease Neuroimaging Initiative, "3D characterization of brain atrophy in Alzheimer's disease and mild cognitive impairment using tensor-based morphometry.," *Neuroimage*, vol. 41, no. 1, pp. 19–34, May 2008.

[3] R. S. J. Frackowiak, K. J. Friston, C. D. Frith, R. J. Dolan, C. J. Price, S. Zeki, J. T. Ashburner, and W. D. Penny, *Human brain function, 2nd Edition*, Elsevier, 2004.

[4] I. Yanovsky, A. D. Leow, S. Lee, S. J. Osher, and P. M. Thompson, "Comparing registration methods for mapping brain change using tensor-based morphometry.," *Med Image Anal*, vol. 13, no. 5, pp. 679–700, Oct 2009.

[5] M. Targosz-Gajniak, J. Siuda, S. Ochudlo, and G. Opala, "Cerebral white matter lesions in patients with dementia - from MCI to severe Alzheimer's disease.," *J Neurol Sci*, vol. 283, no. 1-2, pp. 79–82, Aug 2009.

[6] M. Alegret, G. Vinyes-Junqué, M. Boada, P. Martínez-Lage, G. Cuberas, A. Espinosa, I. Roca, I. Hernández, S. Valero, M. Rosende-Roca, A. Mauleón, J. T. Becker, and L. Tárraga, "Brain perfusion correlates of visuoperceptual deficits in mild cognitive impairment and mild Alzheimer's disease.," *J Alzheimers Dis*, vol. 21, no. 2, pp. 557–567, Jan 2010.

[7] K. Kantarci, C. R. Jack, Y. C. Xu, N. G. Campeau, P. C. O'Brien, G. E. Smith, R. J. Ivnik, B. F. Boeve, E. Kokmen, E. G. Tangalos, and R. C. Petersen, "Mild cognitive impairment and Alzheimer disease: regional diffusivity of water.," *Radiology*, vol. 219, no. 1, pp. 101–107, Apr 2001.

[8] R. J. Radke, S. Andra, O. Al-Kofahi, and B. Roysam, "Image change detection algorithms: a systematic survey," vol. 14, no. 3, pp. 294–307, 2005.

[9] M. Bosc, F. Heitz, J. P. Armspach, I. Namer, D. Gounot, and L. Rumbach, "Automatic change detection in multimodal serial MRI: application to multiple sclerosis lesion evolution.," *Neuroimage*, vol. 20, no. 2, pp. 643–656, Oct 2003.

[10] H. J. Seo and P. Milanfar, "A non-parametric approach to automatic change detection in MRI images of the brain," in *Proc. IEEE Int. Symp. Biomedical Imaging: From Nano to Macro ISBI '09*, 2009, pp. 245–248.

[11] J. Patriarche and B. Erickson, "Part 1. automated change detection and characterization in serial MR studies of brain-tumor patients.," *J Digit Imaging*, vol. 20, no. 3, pp. 203–222, Sep 2007.

[12] L. Lemieux, U. C. Wieshmann, N. F. Moran, D. R. Fish, and S. D. Shorvon, "The detection and significance of subtle changes in mixed-signal brain lesions by serial mri scan matching and spatial normalization.," *Med Image Anal*, vol. 2, no. 3, pp. 227–242, Sep 1998.

[13] F. Bovolo and L. Bruzzone, "A theoretical framework for unsupervised change detection based on change vector analysis in the polar domain," vol. 45, no. 1, pp. 218–236, 2007.

[14] Y. Hsu, H. Nagel, and G. Rekkers, "New likelihood test methods for change detection in image sequences," *Computer Vision Graphics Image Processing*, vol. 26, pp. 73–106, 1984.

[15] S. M. Smith, M. Jenkinson, M.W. Woolrich, C.F. Beckmann, T.E.J. Behrens, H. Johansen-Berg, P.R. Bannister, M. Luca, I. Drobnjak, D.E. Flitney, R.K. Niazy, J. Saunders, J. Vickers, Y. Zhang, N. Stefano, J.M. Brady, and P.M. Matthews, "Advances in functional and structural MR image analysis and implementation as FSL.," *Neuroimage*, vol. 23 Suppl 1, pp. S208–S219, 2004.

[16] M. Jenkinson, P. Bannistera, M. Bradyb, and S. Smith, "Improved optimization for the robust and accurate linear registration and motion correction of brain images," *Neuro*, vol. 17, pp. 825–841, 2002.

[17] S. M. Smith, "Fast robust automated brain extraction.," *Human Brain Mapping,*, vol. 17, no. 3, pp. 143–155, November 2002.

[18] Y. Zhang, M. Brady, and S. Smith, "Segmentation of brain mr images through a hidden markov random field model and the expectation-maximization algorithm.," *IEEE Trans Med Imaging*, vol. 20, no. 1, pp. 45–57, Jan 2001.

[19] L. Ibanez, W. Schroeder, L. Ng, and J. Cates, *The ITK Software Guide*, "Kitware, Inc.", http://www.itk.org/ItkSoftwareGuide.pdf, second edition, 2003.

[20] S. Shen, A. J. Szameitat, and A. Sterr, "Detection of infarct lesions from single MRI modality using inconsistency between voxel intensity and spatial location—a 3-D automatic approach," *IEEE Transactions on Information Technology in Biomedicine*, vol. 12, no. 4, pp. 532–540, 2008.

[21] D.G. Altman, *Practical Statistics for Medical Research*, London England: Chapman and Hall, 1991.

[22] J. J. Bartko, "Measurement and reliability: statistical thinking considerations.," *Schizophr Bull*, vol. 17, no. 3, pp. 483–489, 1991.